Letter

Engineering rich two-dimensional higher-order topological phases by flux and periodic driving

Ming-Jian Gao and Jun-Hong An*

Key Laboratory of Quantum Theory and Applications of MoE, Lanzhou Center for Theoretical Physics, and Key Laboratory of Theoretical Physics of Gansu Province, Lanzhou University, Lanzhou 730000, China

(Received 8 September 2023; accepted 27 November 2023; published 8 December 2023)

Nodal-line semimetals are commonly believed to exist in $\mathcal{PT}$ symmetric or mirror-rotation symmetric systems. Here, we find a flux-induced parameter-dimensional second-order nodal-line semimetal (SONLS) in a two-dimensional system without $\mathcal{PT}$ and mirror-rotation symmetries. It has coexisting hinge Fermi arcs and drumhead surface states. Meanwhile, we discover a flux-induced second-order topological insulator (SOTI). We then propose a Floquet engineering scheme to create exotic parameter-dimensional hybrid-order nodal-line semimetals with abundant nodal-line structures and widely tunable numbers of corner states in a SONLS and SOTI, respectively. Our results break the perception of SONLSs and supply a convenient way to artificially synthesize exotic topological phases by periodic driving.

DOI: 10.1103/PhysRevB.108.L241402

Introduction. As one of the most actively expanding fields in physics, topological phases of matter not only enrich the paradigm of condensed matter physics, but also have a profound impact on quantum technologies [1–5]. Featuring unique Fermi arcs and gapless bulk bands, Dirac [6–14], Weyl [15–23], and nodal-line [24–29] semimetals have exhibited novel transport phenomena due to their chiral anomaly, such as chiral negative magnetoresistance and high carrier mobility [30–33]. Two-dimensional (2D) topological semimetals have been proposed due to their potential applications in semiconductor integrated circuits [34–36]. The finding of higher-order topological phases opens up a frontier of topological physics [37–55]. Second-order topological insulators (SOTIs) are characterized by a corner state in 2D or hinge states in three-dimensional (3D) systems and have fantastic applications [56]. Second-order nodal-line semimetals (SONLSs) with coexisting hinge Fermi arcs and drumhead surface states [52–54] have been predicted. Yet, the general ways of inducing SONLSs and SOTIs are scarce.

It is generally believed that nodal-line semimetals need the protection of either mirror-rotation or $\mathcal{PT}$ symmetry [57]. SONLSs also have been predicted in $\mathcal{PT}$ [51–53] and mirror-rotation [54] symmetric systems. An open question is whether SONLSs could exist without these symmetries. Meanwhile, one of the difficulties in the application of topological phases is that the ways to control various interactions in static systems are limited because their features could not be adjusted once they are fabricated. Coherent control via the periodic driving of external fields, dubbed Floquet engineering, has become a versatile tool in creating novel topological phases in systems of ultracold atoms [58,59], photonics [60], and superconductor qubits [61]. Many intriguing phases unavailable in static systems have been generated by periodic driving in a controllable manner [62–71]. A natural question is if whether, in order to facilitate the exploration of their applications, we can realize a free tunability and conversion of the nodal-line structures and the topological phases of SONLSs and SOTIs by Floquet engineering.

We here investigate the flux-induced higher-order 2D topological phases and their Floquet engineering. An exotic flux-induced parameter-dimensional SONLS, with the third dimension simulated by one system parameter, is discovered in our 2D system with neither $\mathcal{PT}$ nor mirror-rotation symmetry. Enriching the family of 2D topological phases, this phase can be readily generalized to the 3D case. We also find a flux-induced SOTI as a by-product. We further reveal the wide tunability of the nodal-line structures and the topological phases of the SONLSs and SOTIs by Floquet engineering. Hybrid-order nodal-line semimetals, fruitful nodal-line structures, and exotic topological phases with widely tunable numbers of zero- and π/T-mode corner states are created easily by applying a periodic driving. Highlighting the flux and Floquet engineering as two convenient ways to explore exotic higher-order topological phases, our result enriches controllability in topological physics.

Flux-induced second-order topological phases. Conventionally, nodal-line semimetals exist in the systems with either $\mathcal{PT}$ or mirror-rotation symmetry [57]. We explore whether these symmetries are a prerequisite for forming nodal-line semimetals. For this purpose, we consider a system of spinless fermions moving on a square lattice [see Fig. 1(a)]. Its momentum-space Hamiltonian reads $\hat{H}=\sum_{\mathbf{k}}\hat{C}_{\mathbf{k}}^\dagger[\mathcal{H}_0(\mathbf{k})+\mathcal{H}_1(\mathbf{k})]\hat{C}_{\mathbf{k}}$ with $\hat{C}_{\mathbf{k}}^\dagger=(\hat{C}_{\mathbf{k},1}^\dagger\ \hat{C}_{\mathbf{k},2}^\dagger\ \hat{C}_{\mathbf{k},3}^\dagger\ \hat{C}_{\mathbf{k},4}^\dagger)$ and

$$\mathcal{H}_j(\mathbf{k})=\begin{pmatrix}0 & d_j(\mathbf{k})\\ d_j^\dagger(\mathbf{k}) & 0\end{pmatrix}\quad (j=0,1),\tag{1}$$

where $d_0(\mathbf{k})=(\gamma_x+\lambda\cos k_x)\tau_0-i\lambda\sin k_x\tau_x-i(\gamma_y+\lambda\cos k_y)\tau_y+i\lambda\sin k_x\tau_z$, with τ_i being Pauli matrices and τ_0 being the identity matrix. $\gamma_{x/y}$ is the intercell hopping rate and λ is the nearest-neighbor intercell hopping rate. Since it is a

*anjhong@lzu.edu.cn

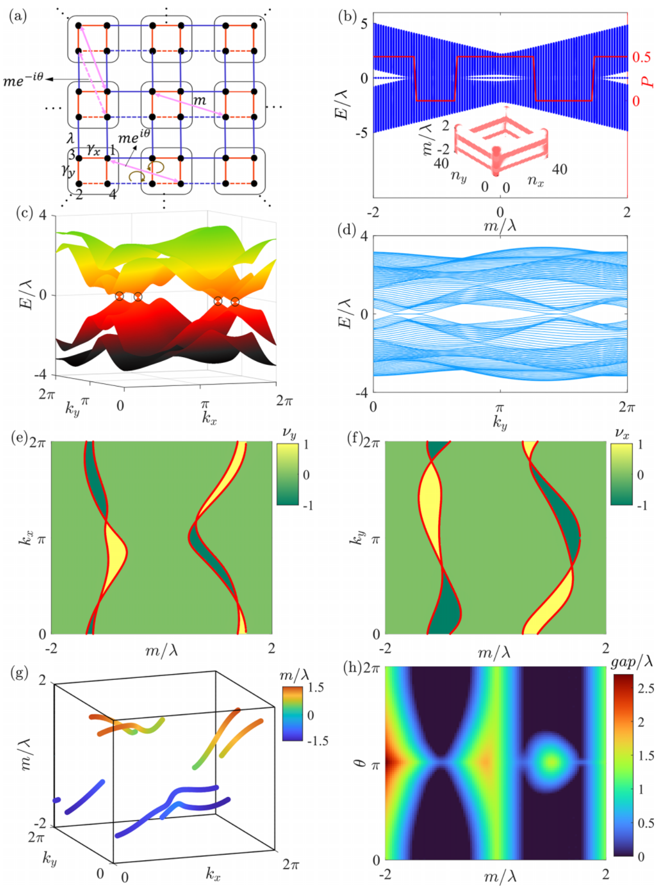

FIG. 1. (a) Scheme of our system. $\gamma_{x/y}$ and λ are the intracell and nearest-neighbor intercell hopping rates, m is the third-order neighbor intercell one, and θ is the flux-induced Peierls phase. The dashed lines denote the hopping rates with a π-phase difference from their solid counterparts. (b) Energy spectrum and quadrupole moment as a function of m. The inset shows coexisting hinge Fermi arcs and drumhead surface states. Energy spectra (c) in momentum space and (d) under the x-direction open boundary condition when $m = 1$. Chiral winding numbers $\nu_{x/y}$ and nodal lines (in red lines) in the (e) k_x-m and (f) k_y-m planes. (g) Nodal lines in the Brillouin zone. (h) Phase diagram described by the bulk gap. We use $\gamma_x = 0.65\lambda$, $\gamma_y = -0.4\lambda$, and $\theta = \pi/2$.

Benalcazar-Bernevig-Hughes model, the system described by $\mathcal{H}_0(\mathbf{k})$ has chiral $\mathcal{S} = \tau_z\sigma_0$, $\mathcal{PT}$, and mirror-rotation symmetries and is a SOTI when $|\gamma_{x/y}| < |\lambda|$ [72]. Inspired by the flux-induced topological phase transition [73], we consider third-order neighbor intercell hopping, which breaks the $\mathcal{P}$ symmetry, and the application of a flux, which further breaks the $\mathcal{PT}$ and mirror-rotation symmetries of $\mathcal{H}_0(\mathbf{k})$. Third-order neighbor intercell hopping is the minimally allowable hopping to cause the overall flux of the lattice to be zero [74]. Then we have $d_1(\mathbf{k}) = m[e^{i(\theta+k_x)}(\tau_x + i\tau_y) + e^{-ik_x}(\tau_x - i\tau_y)]/2 + m[e^{i(\theta-k_y)}(\tau_z - \tau_0) + e^{ik_y}(\tau_0 + \tau_z)]/2$, where m is the third-order neighbor intercell hopping rate and θ is the flux-induced Peierls phase. Only the chiral symmetry is present in $\mathcal{H}(\mathbf{k}) = \mathcal{H}_0(\mathbf{k}) + \mathcal{H}_1(\mathbf{k})$. The absence of $\mathcal{PT}$ symmetry and primitive translations due to $\gamma_x \neq \gamma_y \neq \lambda$ causes our system not to have projective symmetry either [75–79].

It is interesting to find that a parameter-dimensional SONLS, where m is seen as an addition dimension besides $k_{x/y}$, is formed in our 2D system without $\mathcal{PT}$ and mirror-rotation symmetries in the $\gamma_x \neq \gamma_y$ regime. The second-order topology is characterized by the quadrupole moment $P = [\frac{\mathrm{Im}\ln\det\mathcal{F}}{2\pi} - \sum_{\mathbf{n},i;\mathbf{m},j}\frac{A_{\mathbf{n},i;\mathbf{m},j}}{2N_xN_y}]$ mod 1. Here, the elements read $\mathcal{F}_{ab} \equiv \langle\psi_a|e^{i2\pi A/(N_xN_y)}|\psi_b\rangle$, $|\psi_\alpha\rangle$ $(\alpha = a, b)$ satisfying $\hat{H}|\psi_\alpha\rangle = E_\alpha|\psi_\alpha\rangle$ and $E_\alpha < 0$ are the occupied eigenstates, and the coordinate $A_{\mathbf{n},i;\mathbf{m},j} = n_xn_y\delta_{\mathbf{nm}}\delta_{ij}$ with $i, j = 1, \dots, 4$ being the sublattices and $n_{x,y}$ being the numbers of the unit cell [80,81]. The energy spectrum under the open boundary condition in Fig. 1(b) shows that fourfold degenerate zero-mode corner states signified by $P = 0.5$ are formed. In the band-closing parameter regime with $P = 0$, the dispersion relation exhibits four Weyl points [see Fig. 1(c)]. Its energy spectrum in the y-direction periodic boundary condition reveals that a flat band is present between each pair of Weyl points [see Fig. 1(d)]. It is remarkable to find that the flat band is nontrivial in first-order topology, which can be characterized by the winding number [3,82]

$$\nu_p = \frac{1}{4\pi i}\int_{-\pi}^{\pi}\mathrm{Tr}[\mathcal{S}\mathcal{Q}(\mathbf{k})\partial_{k_p}\mathcal{Q}(\mathbf{k})]dk_p. \tag{2}$$

Here, $p = x, y$ and $\mathcal{Q}(\mathbf{k}) = \sum_{l=1,2}[|u_{-l}(\mathbf{k})\rangle\langle u_{-l}(\mathbf{k})| - |u_l(\mathbf{k})\rangle\langle u_l(\mathbf{k})|]$, with $|u_l(\mathbf{k})\rangle$ satisfying $\mathcal{H}(\mathbf{k})|u_l(\mathbf{k})\rangle = E_l(\mathbf{k})|u_l(\mathbf{k})\rangle$. Figures 1(e) and 1(f) indicate that the band-closing regimes in Fig. 1(b) hold nontrivial first-order topology, whose boundaries form the nodal lines. The regions with a nonzero $\nu_{x/y}$ enclosed by the nodal lines are the drumhead surfaces. Separating the first- and second-order phases, such nodal lines are in the second-order type, whose distribution in the m-parametrized Brillouin zone is shown in Fig. 1(g). Combining P and $\nu_{x/y}$, we conclude that a SONLS with a coexisting first-order flat band, which plays the role of the drumhead surface states, and second-order hinge states are formed in our m-parametrized 2D system. The inset of Fig. 1(b) shows the coexisting hinge Fermi arcs and the drumhead surface states. The phase diagram of the SONLS in different θ is given in Fig. 1(h), where the nodal lines exist in the gapless regimes. Our parameter-dimensional SONLS is different from Refs. [51–54] and refreshes one's general belief that nodal-line semimetals need $\mathcal{PT}$ or mirror-rotation symmetry [57]. It enriches our understanding of the 2D topological phase and provides insights for applying 2D materials in quantum devices.

Besides the SONLS, the flux in our system can also induce a SOTI. When $\theta = \pi$ and $\gamma_x = \gamma_y \equiv \gamma$, the time-reversal $\mathcal{T} = K$, with K being the complex conjugation, the spatial inversion $\mathcal{P} = \tau_0\sigma_y$, and the mirror-rotation $\mathcal{M}_{xy} = [(\tau_0 + \tau_z)\sigma_x - (\tau_z - \tau_0)\sigma_z]/2$ symmetries are recovered. Its topology is described by $\mathcal{H}(k, k)$ along the high-symmetry line $k_x = k_y \equiv k$, which is diagonalized into diag$[\mathcal{H}^+(k), \mathcal{H}^-(k)]$ with $\mathcal{H}^\pm(k) = \mathbf{h}^\pm\cdot\sigma$ and $\mathbf{h}^\pm = \sqrt{2}[\gamma + (\lambda + m)\cos k, \pm(\lambda + m)\sin k, 0]$. Thus, the bands coalesce when $|\gamma| = |\lambda + m|$. It exhibits a SOTI characterized by the mirror-graded winding number $W = W_+ - W_-$ [83], where $W_\pm = \frac{i}{2\pi}\int_0^{2\pi}\langle u_\pm(k)|\partial_k|u_\pm(k)\rangle dk$ and $|u_\pm(k)\rangle$ is the eigenstate of $\mathcal{H}^\pm(k)$. The energy spectrum under the open boundary condition in Fig. 2(a) and the probability

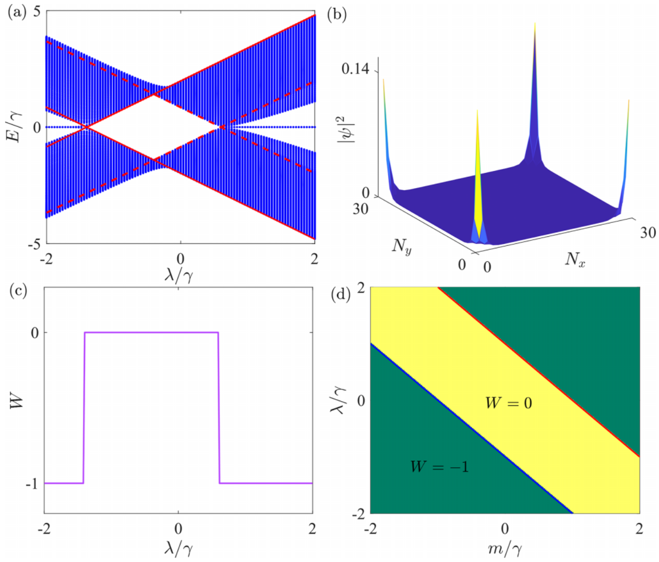

FIG. 2. (a) Energy spectrum and (c) mirror-graded winding number W in different λ when $m = 0.4\gamma$. The red solid (dashed) lines are the dispersion relation along the high-symmetry line $k = 0$ (π). (b) Distribution of the zero-mode state. (d) Phase diagram described by W. We use $\theta = \pi$.

distribution of the zero-mode states in Fig. 2(b) show that the system has fourfold degenerate corner states signified by $W = -1$ of Fig. 2(c) when $\lambda > \gamma - m$ and $\lambda < -(\gamma + m)$. The phase diagram in Fig. 2(d) verifies that the SOTI is present when $|\gamma| < |\lambda + m|$.

Floquet engineering. Determined by the intrinsic parameters, the topological features and the nodal-line structures cannot be changed in static systems, where the hopping parameters are fixed. We propose to conveniently control the topological features and generate rich nodal-line structures by Floquet engineering. First, we consider that the Peierls phase θ is periodically driven as

$$\theta(t) = \begin{cases} \theta_1, & t \in [nT, nT + T_1), \\ \theta_2, & t \in [nT + T_1, (n+1)T), \end{cases} n \in \mathbb{Z}, \quad (3)$$

where $T = T_1 + T_2$ is the driving period. The periodic system $\hat{H}(t)$ does not have an energy spectrum because its energy is not conserved. The Floquet theorem defines an effective Hamiltonian $\hat{H}_{\rm eff} = \frac{i}{T} \ln \hat{U}_T$ from the evolution operator $\hat{U}_T = \mathbb{T} e^{-i\int_0^T \hat{H}(t)dt}$. The eigenvalues of $\hat{H}_{\rm eff}$ are called quasienergies [84,85]. The topological feature of the periodic system is defined in the quasienergy spectrum. Applying the Floquet theorem in our system, we have $\mathcal{H}_{\rm eff}(\mathbf{k}) = \frac{i}{T} \ln[e^{-i\mathcal{H}_2(\mathbf{k})T_2} e^{-i\mathcal{H}_1(\mathbf{k})T_1}]$, where $\mathcal{H}_j(\mathbf{k})$ is the Hamiltonian with θ replaced by θ_j.

The topological phase transition of the periodic system occurs not only at a zero quasienergy gap but also at the π/T one [54,71,86], which causes the inadequacy of the static characterization of the topological phase. We can establish a complete description to the rich emergent topological phases in our periodic system on $\mathcal{H}_{\rm eff}(\mathbf{k})$. $\mathcal{H}_{\rm eff}(\mathbf{k})$ does not inherit the chiral symmetry of $\mathcal{H}(\mathbf{k})$ due to $[\mathcal{H}_1(\mathbf{k}), \mathcal{H}_2(\mathbf{k})] \neq 0$. However, the winding number characterizing the first-order topology requires chiral

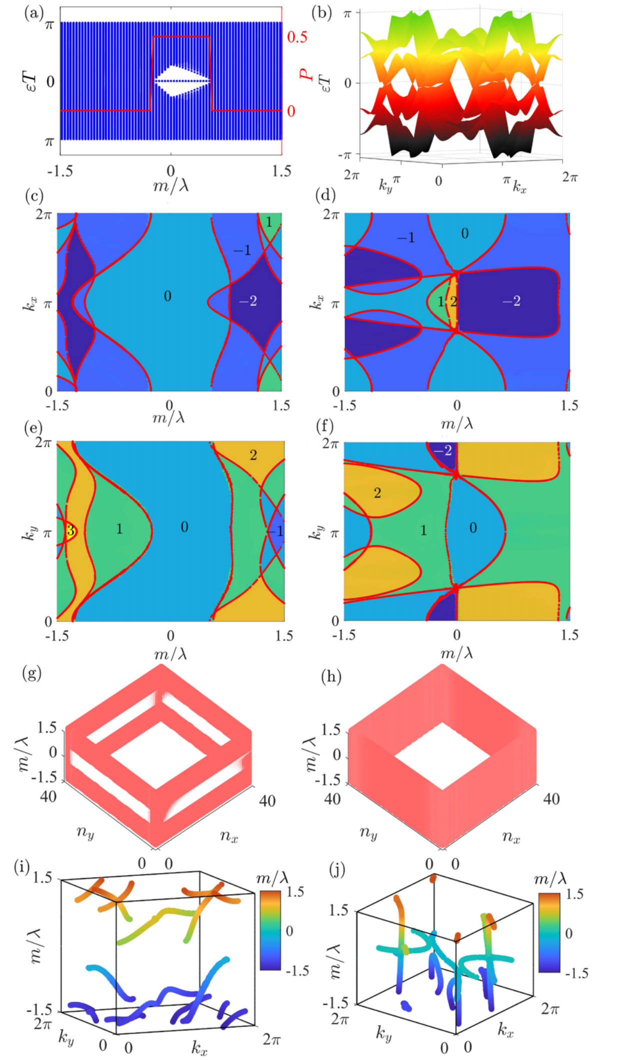

FIG. 3. (a) Quasienergy spectrum and quadrupole moment of the periodic system. (b) Dispersion relation when $m = 1.2\lambda$. Chiral winding numbers (c) ν_x^0, (d) $\nu_y^{\pi/T}$, (e) ν_x^0, and (f) $\nu_y^{\pi/T}$ in the $k_{x/y}$-m planes. (g) Coexisting hinge Fermi arcs and drumhead surface states in the zero mode and (h) pure drumhead surface states in the π/T mode. (i) Zero- and (j) π/T-mode nodal lines in the Brillouin zone. We use $\gamma_x = 0.65\lambda$, $\gamma_y = -0.4\lambda$, $\theta_1 = 0$, $\theta_2 = \pi$, $T_1 = \lambda^{-1}$, and $T_2 = 1.5\lambda^{-1}$.

symmetry. We recover the chiral symmetry by making two unitary transformations $G_l(\mathbf{k}) = e^{i(-1)^l \mathcal{H}_l(\mathbf{k})T_l/2}$ ($l = 1, 2$), which do not change the quasienergy spectrum, and obtain $\widetilde{\mathcal{H}}_{{\rm eff},l}(\mathbf{k}) = iT^{-1} \ln[G_l(\mathbf{k}) U_T(\mathbf{k}) G_l^\dagger(\mathbf{k})]$. Then the two winding numbers ν_l defined in the chirally symmetric $\widetilde{\mathcal{H}}_{{\rm eff},l}(\mathbf{k})$ can be calculated in a similar manner as Eq. (2). The first-order topology of $\mathcal{H}_{\rm eff}(\mathbf{k})$ at the quasienergies α/T, with $\alpha = 0$ or π, relates to ν_l as $\nu^{\alpha/T} = (\nu_1 + e^{i\alpha}\nu_2)/2$ [65]. The number of α/T-mode drumhead surface states is equal to $2|\nu^{\alpha/T}|$. The second-order topological phase is also characterized by P.

We observe two typical regimes from the quasienergy spectrum of $\mathcal{H}_{\rm eff}(\mathbf{k})$ in different m in Fig. 3(a): One has closed quasienergy gaps and the other has gapped zero-mode states. The second-order corner states signified by $P = 0.5$ are present in the regime with the gapped zero-mode states.

Figure 3(b) reveals that the band-touching form becomes more complicated than the static case in Fig. 1(c), which endows us with sufficient room to adjust the nodal-line structure and the number of the drumhead surface states by Floquet engineering. The first-order topological phase is characterized by the winding number $\nu_{x/y}^{\alpha/T}$ in Figs. 3(c)–3(f) in the regimes with a closed quasienergy gap. The regions with a nonzero $\nu_{x/y}^{\alpha/T}$ enclosed by the nodal lines are just the drumhead surfaces, whose boundaries match well with the projection of the nodal lines [see the red lines in Figs. 3(c)–3(f)]. First-order topological phases that are richer than the static case in Figs. 1(e) and 1(f) are created by periodic driving. In particular, the phases of widely tunable $\nu_{x/y}^{0}$ from -2 to 3 and $\nu_{x/y}^{\pi/T}$ from -2 to 2 absent in the static case are present. Combining the second-order topological phase in Fig. 3(a) with the first-order one in Figs. 3(c)–3(f), our periodic system exhibits an m-parametrized hybrid-order nodal-line semimetal. It has coexisting second-order nodal lines in the zero mode, which host the hinge Fermi arcs and the drumhead surface states in Fig. 3(g), and the first-order ones in the π/T mode, which host the pure drumhead surface states in Fig. 3(h). The distributions of the zero- and π/T-mode nodal lines in our periodic system in Figs. 3(i) and 3(j) show dramatic differences from the static case in Fig. 1(g). First, the number of zero-mode nodal lines increases. Second, the π/T-mode nodal lines are interwoven to form a nodal net at the $m = 0.1\lambda$ plane and nodal loops at m from -1.5λ to -1.2λ. Such rich nodal-line structures confirm the diverse topological phases in Figs. 3(c)–3(f), which are difficult to realize in static systems. Thus, our result reveals that the topological phases and the nodal-line structures can be well controlled by Floquet engineering.

Next, we study the rich Floquet SOTIs by choosing $\gamma_x = \gamma_y$. Setting $\theta = \pi$ to preserve the $\mathcal{PT}$ and mirror-rotation symmetries, the driving is applied on m as

$$m(t) = \begin{cases} m_1, & t \in [nT, nT + T_1), \\ m_2, & t \in [nT + T_1, (n+1)T). \end{cases} \tag{4}$$

$\mathcal{H}_{\text{eff}}(\mathbf{k})$ is derived in the same manner as above. First, the topological description can be established on $\mathcal{H}_{\text{eff}}(\mathbf{k})$. After making two unitary transformations $G_l(\mathbf{k})$ to $\mathcal{H}_{\text{eff}}(\mathbf{k})$ to recover the chiral symmetry, we calculate the winding numbers W_l from $\widetilde{\mathcal{H}}_{\text{eff},l}(\mathbf{k})$. The SOTIs in the quasienergy gaps α/T are characterized by the mirror-graded winding number $W_{\alpha/T} = (W_1 + e^{i\alpha} W_2)/2$. The number of α/T-mode corner states is equal to $4|W_{\alpha/T}|$. Second, it is derived from $\mathcal{H}_{\text{eff}}(\mathbf{k})$ that a phase transition occurs for $\mathbf{k}$ and the parameters satisfying either [65,71,86]

$$T_j E_j = c_j \pi, \tag{5}$$

or

$$\begin{aligned} \underline{\mathbf{h}}_1 \cdot \underline{\mathbf{h}}_2 &= \pm 1, \\ T_1 E_1 \pm T_2 E_2 &= c\pi, \end{aligned} \tag{6}$$

with $\underline{\mathbf{h}}_j \equiv \mathbf{h}_j / |\mathbf{h}_j|$, at zero quasienergy (or π/T) when c_j are integers with the same (or different) parity and c is an even (or odd) number. Using Eqs. (5) and (6) on $\mathcal{H}^{\pm}(k)$, we obtain the phase boundaries as follows. Equation (5) results in a phase transition that occurs at $\mathbf{k}$ satisfying

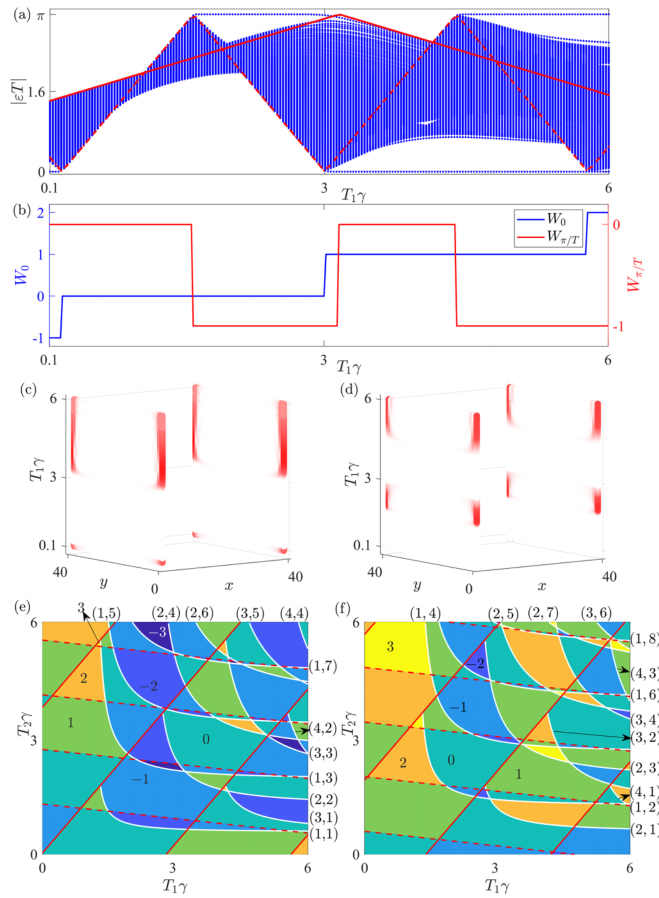

FIG. 4. (a) Quasienergy spectrum and (b) mirror-graded winding number $W_{\alpha/T}$ of the periodic system when $T_2 = 0.3\gamma^{-1}$. The red solid (dashed) line is the dispersion relation along the high-symmetry line $k = 0$ (π). Distributions of the (c) zero- and (d) π/T-mode states in different T_1. Phase diagram described by (e) W_0 and (f) $W_{\pi/T}$. The white lines are from Eqs. (7) with the labeled (c_1, c_2). The red solid lines are from Eqs. (8) with $c_{\pi,-} = -2, 0, 2, 4$ in (e), $c_{\pi,-} = -3, -1, 1, 3$ in (f), and the red dashed line with $c_{0,+} = 2, 4, 6, 8$ in (e), $c_{0,+} = 1, 3, 5, 7, 9$ in (f). We use $\lambda = 0$, $m_1 = -0.6\gamma$, and $m_2 = 2.2\gamma$.

$$\sqrt{2}[\gamma^2 + (\lambda + m_j)^2 + 2\gamma(\lambda + m_j)\cos k]^{\frac{1}{2}} T_j = c_j \pi. \tag{7}$$

$\underline{\mathbf{h}}_1 \cdot \underline{\mathbf{h}}_2 = \pm 1$ in Eq. (6) needs the high-symmetry line $k \equiv \bar{k} = 0$ or π. Thus, the phase transition occurs at

$$\sqrt{2}[|\gamma + (\lambda + m_1)e^{i\bar{k}}|T_1 \pm |\gamma + (\lambda + m_2)e^{i\bar{k}}|T_2] = c_{\bar{k},\pm}\pi. \tag{8}$$

Figures 4(a) and 4(b) show the quasienergy spectrum and mirror-graded winding numbers $W_{\alpha/T}$ of $\mathcal{H}_{\text{eff}}(\mathbf{k})$. It is seen that the α/T-mode corner states are well described by $W_{\alpha/T}$. Their probability distributions in Figs. 4(c) and 4(d) confirm that a SOTI is formed in both the zero and π/T modes. To give a global picture of the SOTI, we plot in Figs. 4(e) and 4(f) the phase diagram characterized by $W_{\alpha/T}$ in the T_1-T_2 plane. Much richer SOTIs with a widely tunable number of zero- and π/T-mode corner states than the static case in Fig. 2(d) are created by periodic driving. The phase boundaries are well described by the analytical conditions of Eqs. (7) and (8). All the results indicate that periodic driving assisted by the flux offers us a useful way to generate exotic second-order topological phases.

Discussion and conclusion. Our result is generalizable to the 3D case. Replacing m in Eq. (1) by $\chi(k_z) = m + \xi\cos(k_z)$, with ξ being the interlayer hopping rate, we obtain a 3D model. It can be verified that this 3D model still does not have $\mathcal{PT}$ and mirror-rotation symmetries, but it possesses the topological phase of a SONLS. The steplike driving scheme can be generalized to any type of driving protocol. The higher-order semimetals have been simulated in some materials [48], Josephson junctions [87], and realized in classical acoustic metamaterials [88,89]. SOTIs have been realized in various systems [90–96]. Floquet engineering has been used to design novel topological phases in several platforms [60,61,97–102]. The progress indicates that our result is realizable in state-of-the-art experiments.

In summary, we have proposed a flux-induced parameter-dimensional SONLS in a system without $\mathcal{PT}$ and mirror-rotation symmetries. It enriches our understanding of the 2D topological phase and provides different possibilities for the application of 2D materials. We have also found that an exotic hybrid-order nodal-line semimetal and abundant nodal-line structures are created easily by periodic driving. We have also discovered a flux-induced SOTI and explored its wide tunability by Floquet engineering. Our work enriches the family of topological semimetals and provides a convenient way to reduce the practical difficulties in adjusting nodal-line structures, Fermi arcs, the drumhead surface states of SONLSs, and the numbers of corner states of SOTIs in static systems. This significantly expands the application of topological phases and increases their controllability.

Acknowledgment. The work is supported by the National Natural Science Foundation (Grants No. 12275109, No. 12247101, and No. 11834005).

[1] M. Z. Hasan and C. L. Kane, *Colloquium:* Topological insulators, Rev. Mod. Phys. **82**, 3045 (2010).

[2] X.-L. Qi and S.-C. Zhang, Topological insulators and superconductors, Rev. Mod. Phys. **83**, 1057 (2011).

[3] C.-K. Chiu, J. C. Y. Teo, A. P. Schnyder, and S. Ryu, Classification of topological quantum matter with symmetries, Rev. Mod. Phys. **88**, 035005 (2016).

[4] N. P. Armitage, E. J. Mele, and A. Vishwanath, Weyl and Dirac semimetals in three-dimensional solids, Rev. Mod. Phys. **90**, 015001 (2018).

[5] B. Q. Lv, T. Qian, and H. Ding, Experimental perspective on three-dimensional topological semimetals, Rev. Mod. Phys. **93**, 025002 (2021).

[6] Z. K. Liu, B. Zhou, Y. Zhang, Z. J. Wang, H. M. Weng, D. Prabhakaran, S.-K. Mo, Z. X. Shen, Z. Fang, X. Dai, Z. Hussain, and Y. L. Chen, Discovery of a three-dimensional topological Dirac semimetal, Na_3Bi, Science **343**, 864 (2014).

[7] M. Neupane, S.-Y. Xu, R. Sankar, N. Alidoust, G. Bian, C. Liu, I. Belopolski, T.-R. Chang, H.-T. Jeng, H. Lin, A. Bansil, F. Chou, and M. Z. Hasan, Observation of a three-dimensional topological Dirac semimetal phase in high-mobility Cd_3As_2, Nat. Commun. **5**, 3786 (2014).

[8] S. Borisenko, Q. Gibson, D. Evtushinsky, V. Zabolotnyy, B. Büchner, and R. J. Cava, Experimental realization of a three-dimensional Dirac semimetal, Phys. Rev. Lett. **113**, 027603 (2014).

[9] S.-Y. Xu, C. Liu, S. K. Kushwaha, R. Sankar, J. W. Krizan, I. Belopolski, M. Neupane, G. Bian, N. Alidoust, T.-R. Chang, H.-T. Jeng, C.-Y. Huang, W.-F. Tsai, H. Lin, P. P. Shibayev, F.-C. Chou, R. J. Cava, and M. Z. Hasan, Observation of Fermi arc surface states in a topological metal, Science **347**, 294 (2015).

[10] S. M. Young, S. Zaheer, J. C. Y. Teo, C. L. Kane, E. J. Mele, and A. M. Rappe, Dirac semimetal in three dimensions, Phys. Rev. Lett. **108**, 140405 (2012).

[11] R. Y. Chen, Z. G. Chen, X.-Y. Song, J. A. Schneeloch, G. D. Gu, F. Wang, and N. L. Wang, Magnetoinfrared spectroscopy of Landau levels and Zeeman splitting of three-dimensional massless Dirac fermions in $ZrTe_5$, Phys. Rev. Lett. **115**, 176404 (2015).

[12] Y. Liu, X. Yuan, C. Zhang, Z. Jin, A. Narayan, C. Luo, Z. Chen, L. Yang, J. Zou, X. Wu, S. Sanvito, Z. Xia, L. Li, Z. Wang, and F. Xiu, Zeeman splitting and dynamical mass generation in Dirac semimetal $ZrTe_5$, Nat. Commun. **7**, 12516 (2016).

[13] S. M. Young and C. L. Kane, Dirac semimetals in two dimensions, Phys. Rev. Lett. **115**, 126803 (2015).

[14] T.-R. Chang, S.-Y. Xu, D. S. Sanchez, W.-F. Tsai, S.-M. Huang, G. Chang, C.-H. Hsu, G. Bian, I. Belopolski, Z.-M. Yu, S. A. Yang, T. Neupert, H.-T. Jeng, H. Lin, and M. Z. Hasan, Type-II symmetry-protected topological Dirac semimetals, Phys. Rev. Lett. **119**, 026404 (2017).

[15] X. Wan, A. M. Turner, A. Vishwanath, and S. Y. Savrasov, Topological semimetal and Fermi-arc surface states in the electronic structure of pyrochlore iridates, Phys. Rev. B **83**, 205101 (2011).

[16] S.-Y. Xu, I. Belopolski, N. Alidoust, M. Neupane, G. Bian, C. Zhang, R. Sankar, G. Chang, Z. Yuan, C.-C. Lee, S.-M. Huang, H. Zheng, J. Ma, D. S. Sanchez, B. Wang, A. Bansil, F. Chou, P. P. Shibayev, H. Lin, S. Jia *et al.*, Discovery of a Weyl fermion semimetal and topological Fermi arcs, Science **349**, 613 (2015).

[17] B. Q. Lv, H. M. Weng, B. B. Fu, X. P. Wang, H. Miao, J. Ma, P. Richard, X. C. Huang, L. X. Zhao, G. F. Chen, Z. Fang, X. Dai, T. Qian, and H. Ding, Experimental discovery of Weyl semimetal TaAs, Phys. Rev. X **5**, 031013 (2015).

[18] X. Huang, L. Zhao, Y. Long, P. Wang, D. Chen, Z. Yang, H. Liang, M. Xue, H. Weng, Z. Fang, X. Dai, and G. Chen, Observation of the chiral-anomaly-induced negative magnetoresistance in 3D Weyl semimetal TaAs, Phys. Rev. X **5**, 031023 (2015).

[19] T. Nguyen, F. Han, N. Andrejevic, R. Pablo-Pedro, A. Apte, Y. Tsurimaki, Z. Ding, K. Zhang, A. Alatas, E. E. Alp, S. Chi, J. Fernandez-Baca, M. Matsuda, D. A. Tennant, Y. Zhao,

Z. Xu, J. W. Lynn, S. Huang, and M. Li, Topological singularity induced chiral Kohn anomaly in a Weyl semimetal, Phys. Rev. Lett. **124**, 236401 (2020).

[20] S.-M. Huang, S.-Y. Xu, I. Belopolski, C.-C. Lee, G. Chang, B. Wang, N. Alidoust, G. Bian, M. Neupane, C. Zhang, S. Jia, A. Bansil, H. Lin, and M. Z. Hasan, A Weyl fermion semimetal with surface Fermi arcs in the transition metal monopnictide TaAs class, Nat. Commun. **6**, 7373 (2015).

[21] L. X. Yang, Z. K. Liu, Y. Sun, H. Peng, H. F. Yang, T. Zhang, B. Zhou, Y. Zhang, Y. F. Guo, M. Rahn, D. Prabhakaran, Z. Hussain, S. K. Mo, C. Felser, B. Yan, and Y. L. Chen, Weyl semimetal phase in the non-centrosymmetric compound TaAs, Nat. Phys. **11**, 728 (2015).

[22] C. Shekhar, A. K. Nayak, Y. Sun, M. Schmidt, M. Nicklas, I. Leermakers, U. Zeitler, Y. Skourski, J. Wosnitza, Z. Liu, Y. Chen, W. Schnelle, H. Borrmann, Y. Grin, C. Felser, and B. Yan, Extremely large magnetoresistance and ultrahigh mobility in the topological Weyl semimetal candidate NbP, Nat. Phys. **11**, 645 (2015).

[23] S.-Y. Xu, N. Alidoust, I. Belopolski, Z. Yuan, G. Bian, T.-R. Chang, H. Zheng, V. N. Strocov, D. S. Sanchez, G. Chang, C. Zhang, D. Mou, Y. Wu, L. Huang, C.-C. Lee, S.-M. Huang, B. Wang, A. Bansil, H.-T. Jeng, T. Neupert *et al.*, Discovery of a Weyl fermion state with Fermi arcs in niobium arsenide, Nat. Phys. **11**, 748 (2015).

[24] Z. Yan, R. Bi, H. Shen, L. Lu, S.-C. Zhang, and Z. Wang, Nodal-link semimetals, Phys. Rev. B **96**, 041103(R) (2017).

[25] C. Li, C. M. Wang, B. Wan, X. Wan, H.-Z. Lu, and X. C. Xie, Rules for phase shifts of quantum oscillations in topological nodal-line semimetals, Phys. Rev. Lett. **120**, 146602 (2018).

[26] N. Xu, Y. T. Qian, Q. S. Wu, G. Autès, C. E. Matt, B. Q. Lv, M. Y. Yao, V. N. Strocov, E. Pomjakushina, K. Conder, N. C. Plumb, M. Radovic, O. V. Yazyev, T. Qian, H. Ding, J. Mesot, and M. Shi, Trivial topological phase of CaAgP and the topological nodal-line transition in $CaAg(P_{1-x}As_x)$, Phys. Rev. B **97**, 161111(R) (2018).

[27] G. Bian, T.-R. Chang, H. Zheng, S. Velury, S.-Y. Xu, T. Neupert, C.-K. Chiu, S.-M. Huang, D. S. Sanchez, I. Belopolski, N. Alidoust, P.-J. Chen, G. Chang, A. Bansil, H.-T. Jeng, H. Lin, and M. Z. Hasan, Drumhead surface states and topological nodal-line fermions in $TlTaSe_2$, Phys. Rev. B **93**, 121113(R) (2016).

[28] R. Yu, H. Weng, Z. Fang, X. Dai, and X. Hu, Topological node-line semimetal and Dirac semimetal state in antiperovskite Cu_3PdN, Phys. Rev. Lett. **115**, 036807 (2015).

[29] Y.-H. Chan, C.-K. Chiu, M. Y. Chou, and A. P. Schnyder, Ca_3P_2 and other topological semimetals with line nodes and drumhead surface states, Phys. Rev. B **93**, 205132 (2016).

[30] S. Jia, S.-Y. Xu, and M. Z. Hasan, Weyl semimetals, Fermi arcs and chiral anomalies, Nat. Mater. **15**, 1140 (2016).

[31] C. R. Rajamathi, U. Gupta, N. Kumar, H. Yang, Y. Sun, V. Süß, C. Shekhar, M. Schmidt, H. Blumtritt, P. Werner, B. Yan, S. Parkin, C. Felser, and C. N. R. Rao, Weyl semimetals as hydrogen evolution catalysts, Adv. Mater. **29**, 1606202 (2017).

[32] Q. Wang, C.-Z. Li, S. Ge, J.-G. Li, W. Lu, J. Lai, X. Liu, J. Ma, D.-P. Yu, Z.-M. Liao, and D. Sun, Ultrafast broadband photodetectors based on three-dimensional Dirac semimetal Cd_3As_2, Nano Lett. **17**, 834 (2017).

[33] F. Han, N. Andrejevic, T. Nguyen, V. Kozii, Q. T. Nguyen, T. Hogan, Z. Ding, R. Pablo-Pedro, S. Parjan, B. Skinner, A. Alatas, E. Alp, S. Chi, J. Fernandez-Baca, S. Huang, L. Fu, and M. Li, Quantized thermoelectric Hall effect induces giant power factor in a topological semimetal, Nat. Commun. **11**, 6167 (2020).

[34] B. Feng, R.-W. Zhang, Y. Feng, B. Fu, S. Wu, K. Miyamoto, S. He, L. Chen, K. Wu, K. Shimada, T. Okuda, and Y. Yao, Discovery of Weyl nodal lines in a single-layer ferromagnet, Phys. Rev. Lett. **123**, 116401 (2019).

[35] B. Feng, B. Fu, S. Kasamatsu, S. Ito, P. Cheng, C.-C. Liu, Y. Feng, S. Wu, S. K. Mahatha, P. Sheverdyaeva, P. Moras, M. Arita, O. Sugino, T.-C. Chiang, K. Shimada, K. Miyamoto, T. Okuda, K. Wu, L. Chen, Y. Yao *et al.*, Experimental realization of two-dimensional Dirac nodal line fermions in monolayer Cu_2Si, Nat. Commun. **8**, 1007 (2017).

[36] B. Guo, W. Miao, V. Huang, A. C. Lygo, X. Dai, and S. Stemmer, Zeeman field-induced two-dimensional Weyl semimetal phase in cadmium arsenide, Phys. Rev. Lett. **131**, 046601 (2023).

[37] W. A. Benalcazar, B. A. Bernevig, and T. L. Hughes, Quantized electric multipole insulators, Science **357**, 61 (2017).

[38] J. Langbehn, Y. Peng, L. Trifunovic, F. von Oppen, and P. W. Brouwer, Reflection-symmetric second-order topological insulators and superconductors, Phys. Rev. Lett. **119**, 246401 (2017).

[39] Z. Song, Z. Fang, and C. Fang, $(d-2)$-dimensional edge states of rotation symmetry protected topological states, Phys. Rev. Lett. **119**, 246402 (2017).

[40] Z. Yan, F. Song, and Z. Wang, Majorana corner modes in a high-temperature platform, Phys. Rev. Lett. **121**, 096803 (2018).

[41] M. Ezawa, Topological switch between second-order topological insulators and topological crystalline insulators, Phys. Rev. Lett. **121**, 116801 (2018).

[42] F. Liu, H.-Y. Deng, and K. Wakabayashi, Helical topological edge states in a quadrupole phase, Phys. Rev. Lett. **122**, 086804 (2019).

[43] R.-X. Zhang, W. S. Cole, X. Wu, and S. Das Sarma, Higher-order topology and nodal topological superconductivity in Fe(Se,Te) heterostructures, Phys. Rev. Lett. **123**, 167001 (2019).

[44] M. J. Park, Y. Kim, G. Y. Cho, and S. B. Lee, Higher-order topological insulator in twisted bilayer graphene, Phys. Rev. Lett. **123**, 216803 (2019).

[45] X.-L. Sheng, C. Chen, H. Liu, Z. Chen, Z.-M. Yu, Y. X. Zhao, and S. A. Yang, Two-dimensional second-order topological insulator in graphdiyne, Phys. Rev. Lett. **123**, 256402 (2019).

[46] A. Tiwari, M.-H. Li, B. A. Bernevig, T. Neupert, and S. A. Parameswaran, Unhinging the surfaces of higher-order topological insulators and superconductors, Phys. Rev. Lett. **124**, 046801 (2020).

[47] Y. Ren, Z. Qiao, and Q. Niu, Engineering corner states from two-dimensional topological insulators, Phys. Rev. Lett. **124**, 166804 (2020).

[48] B. J. Wieder, Z. Wang, J. Cano, X. Dai, L. M. Schoop, B. Bradlyn, and B. A. Bernevig, Strong and fragile topological Dirac semimetals with higher-order Fermi arcs, Nat. Commun. **11**, 627 (2020).

[49] H.-X. Wang, Z.-K. Lin, B. Jiang, G.-Y. Guo, and J.-H. Jiang, Higher-order Weyl semimetals, Phys. Rev. Lett. **125**, 146401 (2020).

[50] S. A. A. Ghorashi, T. Li, and T. L. Hughes, Higher-order Weyl semimetals, Phys. Rev. Lett. **125**, 266804 (2020).

[51] K. Wang, J.-X. Dai, L. B. Shao, S. A. Yang, and Y. X. Zhao, Boundary criticality of $\mathcal{PT}$-invariant topology and second-order nodal-line semimetals, Phys. Rev. Lett. **125**, 126403 (2020).

[52] L. B. Shao, Q. Liu, R. Xiao, S. A. Yang, and Y. X. Zhao, Gauge-field extended $k \cdot p$ method and novel topological phases, Phys. Rev. Lett. **127**, 076401 (2021).

[53] C. Chen, X.-T. Zeng, Z. Chen, Y. X. Zhao, X.-L. Sheng, and S. A. Yang, Second-order real nodal-line semimetal in three-dimensional graphdiyne, Phys. Rev. Lett. **128**, 026405 (2022).

[54] M.-J. Gao, H. Wu, and J.-H. An, Engineering second-order nodal-line semimetals by breaking $\mathcal{PT}$ symmetry and periodic driving, Phys. Rev. B **107**, 035128 (2023).

[55] F. Schindler, A. M. Cook, M. G. Vergniory, Z. Wang, S. S. P. Parkin, B. A. Bernevig, and T. Neupert, Higher-order topological insulators, Sci. Adv. **4**, eaat0346 (2018).

[56] W. Zhang, X. Xie, H. Hao, J. Dang, S. Xiao, S. Shi, H. Ni, Z. Niu, C. Wang, K. Jin, X. Zhang, and X. Xu, Low-threshold topological nanolasers based on the second-order corner state, Light. Sci. Appl. **9**, 109 (2020).

[57] J. Li, H. Wang, and H. Pan, Tunable topological phase transition from nodal-line semimetal to Weyl semimetal by breaking symmetry, Phys. Rev. B **104**, 235136 (2021).

[58] A. Eckardt, *Colloquium:* Atomic quantum gases in periodically driven optical lattices, Rev. Mod. Phys. **89**, 011004 (2017).

[59] F. Meinert, M. J. Mark, K. Lauber, A. J. Daley, and H.-C. Nägerl, Floquet engineering of correlated tunneling in the Bose-Hubbard model with ultracold atoms, Phys. Rev. Lett. **116**, 205301 (2016).

[60] M. C. Rechtsman, J. M. Zeuner, Y. Plotnik, Y. Lumer, D. Podolsky, F. Dreisow, S. Nolte, M. Segev, and A. Szameit, Photonic Floquet topological insulators, Nature (London) **496**, 196 (2013).

[61] P. Roushan, C. Neill, A. Megrant, Y. Chen, R. Babbush, R. Barends, B. Campbell, Z. Chen, B. Chiaro, A. Dunsworth, A. Fowler, E. Jeffrey, J. Kelly, E. Lucero, J. Mutus, P. J. J. OHuo Heng alley, M. Neeley, C. Quintana, D. Sank, A. Vainsencher *et al.*, Chiral ground-state currents of interacting photons in a synthetic magnetic field, Nat. Phys. **13**, 146 (2017).

[62] T.-S. Xiong, J. Gong, and J.-H. An, Towards large-Chern-number topological phases by periodic quenching, Phys. Rev. B **93**, 184306 (2016).

[63] H. Liu, T.-S. Xiong, W. Zhang, and J.-H. An, Floquet engineering of exotic topological phases in systems of cold atoms, Phys. Rev. A **100**, 023622 (2019).

[64] H. Wu and J.-H. An, Floquet topological phases of non-Hermitian systems, Phys. Rev. B **102**, 041119(R) (2020).

[65] H. Wu, B.-Q. Wang, and J.-H. An, Floquet second-order topological insulators in non-Hermitian systems, Phys. Rev. B **103**, L041115 (2021).

[66] L. Li, C. H. Lee, and J. Gong, Realistic Floquet semimetal with exotic topological linkages between arbitrarily many nodal loops, Phys. Rev. Lett. **121**, 036401 (2018).

[67] Y. Peng and G. Refael, Floquet second-order topological insulators from nonsymmorphic space-time symmetries, Phys. Rev. Lett. **123**, 016806 (2019).

[68] H. Hu, B. Huang, E. Zhao, and W. V. Liu, Dynamical singularities of Floquet higher-order topological insulators, Phys. Rev. Lett. **124**, 057001 (2020).

[69] B. Huang and W. V. Liu, Floquet higher-order topological insulators with anomalous dynamical polarization, Phys. Rev. Lett. **124**, 216601 (2020).

[70] T. Nag, V. Juričić, and B. Roy, Hierarchy of higher-order Floquet topological phases in three dimensions, Phys. Rev. B **103**, 115308 (2021).

[71] B.-Q. Wang, H. Wu, and J.-H. An, Engineering exotic second-order topological semimetals by periodic driving, Phys. Rev. B **104**, 205117 (2021).

[72] W. A. Benalcazar, B. A. Bernevig, and T. L. Hughes, Electric multipole moments, topological multipole moment pumping, and chiral hinge states in crystalline insulators, Phys. Rev. B **96**, 245115 (2017).

[73] C.-A. Li, S.-B. Zhang, J. C. Budich, and B. Trauzettel, Transition from metal to higher-order topological insulator driven by random flux, Phys. Rev. B **106**, L081410 (2022).

[74] F. D. M. Haldane, Model for a quantum Hall effect without Landau levels: Condensed-matter realization of the "parity anomaly", Phys. Rev. Lett. **61**, 2015 (1988).

[75] H. Xue, Z. Wang, Y.-X. Huang, Z. Cheng, L. Yu, Y. X. Foo, Y. X. Zhao, S. A. Yang, and B. Zhang, Projectively enriched symmetry and topology in acoustic crystals, Phys. Rev. Lett. **128**, 116802 (2022).

[76] Y. X. Zhao, C. Chen, X.-L. Sheng, and S. A. Yang, Switching spinless and spinful topological phases with projective *PT* symmetry, Phys. Rev. Lett. **126**, 196402 (2021).

[77] T. Li, J. Du, Q. Zhang, Y. Li, X. Fan, F. Zhang, and C. Qiu, Acoustic Möbius insulators from projective symmetry, Phys. Rev. Lett. **128**, 116803 (2022).

[78] Y. X. Zhao, Y.-X. Huang, and S. A. Yang, $\mathbb{Z}_2$-projective translational symmetry protected topological phases, Phys. Rev. B **102**, 161117(R) (2020).

[79] Y. Meng, S. Lin, B.-J. Shi, B. Wei, L. Yang, B. Yan, Z. Zhu, X. Xi, Y. Wang, Y. Ge, S.-q. Yuan, J. Chen, G.-G. Liu, H.-X. Sun, H. Chen, Y. Yang, and Z. Gao, Spinful topological phases in acoustic crystals with projective $\mathcal{PT}$ symmetry, Phys. Rev. Lett. **130**, 026101 (2023).

[80] B. Kang, K. Shiozaki, and G. Y. Cho, Many-body order parameters for multipoles in solids, Phys. Rev. B **100**, 245134 (2019).

[81] W. A. Wheeler, L. K. Wagner, and T. L. Hughes, Many-body electric multipole operators in extended systems, Phys. Rev. B **100**, 245135 (2019).

[82] F. Song, S. Yao, and Z. Wang, Non-Hermitian topological invariants in real space, Phys. Rev. Lett. **123**, 246801 (2019).

[83] T. Liu, Y.-R. Zhang, Q. Ai, Z. Gong, K. Kawabata, M. Ueda, and F. Nori, Second-order topological phases in non-Hermitian systems, Phys. Rev. Lett. **122**, 076801 (2019).

[84] H. Sambe, Steady states and quasienergies of a quantum-mechanical system in an oscillating field, Phys. Rev. A **7**, 2203 (1973).

[85] C. Chen, J.-H. An, H.-G. Luo, C. P. Sun, and C. H. Oh, Floquet control of quantum dissipation in spin chains, Phys. Rev. A **91**, 052122 (2015).

[86] H. Wu and J.-H. An, Non-Hermitian Weyl semimetal and its Floquet engineering, Phys. Rev. B **105**, L121113 (2022).

[87] C.-Z. Li, A.-Q. Wang, C. Li, W.-Z. Zheng, A. Brinkman, D.-P. Yu, and Z.-M. Liao, Reducing electronic transport dimension to topological hinge states by increasing geometry size of Dirac semimetal Josephson junctions, Phys. Rev. Lett. **124**, 156601 (2020).

[88] L. Luo, H.-X. Wang, Z.-K. Lin, B. Jiang, Y. Wu, F. Li, and J.-H. Jiang, Observation of a phononic higher-order Weyl semimetal, Nat. Mater. **20**, 794 (2021).

[89] Q. Wei, X. Zhang, W. Deng, J. Lu, X. Huang, M. Yan, G. Chen, Z. Liu, and S. Jia, Higher-order topological semimetal in acoustic crystals, Nat. Mater. **20**, 812 (2021).

[90] M. Serra-Garcia, V. Peri, R. Süsstrunk, O. R. Bilal, T. Larsen, L. G. Villanueva, and S. D. Huber, Observation of a phononic quadrupole topological insulator, Nature (London) **555**, 342 (2018).

[91] C. W. Peterson, W. A. Benalcazar, T. L. Hughes, and G. Bahl, A quantized microwave quadrupole insulator with topologically protected corner states, Nature (London) **555**, 346 (2018).

[92] F. Schindler, Z. Wang, M. G. Vergniory, A. M. Cook, A. Murani, S. Sengupta, A. Y. Kasumov, R. Deblock, S. Jeon, I. Drozdov, H. Bouchiat, S. Guéron, A. Yazdani, B. A. Bernevig, and T. Neupert, Higher-order topology in bismuth, Nat. Phys. **14**, 918 (2018).

[93] S. Imhof, C. Berger, F. Bayer, J. Brehm, L. W. Molenkamp, T. Kiessling, F. Schindler, C. H. Lee, M. Greiter, T. Neupert, and R. Thomale, Topolectrical-circuit realization of topological corner modes, Nat. Phys. **14**, 925 (2018).

[94] H. Fan, B. Xia, L. Tong, S. Zheng, and D. Yu, Elastic higher-order topological insulator with topologically protected corner states, Phys. Rev. Lett. **122**, 204301 (2019).

[95] J. Wu, X. Huang, J. Lu, Y. Wu, W. Deng, F. Li, and Z. Liu, Observation of corner states in second-order topological electric circuits, Phys. Rev. B **102**, 104109 (2020).

[96] S. Mittal, V. V. Orre, G. Zhu, M. A. Gorlach, A. Poddubny, and M. Hafezi, Photonic quadrupole topological phases, Nat. Photon. **13**, 692 (2019).

[97] F. Mahmood, C.-K. Chan, Z. Alpichshev, D. Gardner, Y. Lee, P. A. Lee, and N. Gedik, Selective scattering between Floquet-Bloch and Volkov states in a topological insulator, Nat. Phys. **12**, 306 (2016).

[98] J. W. McIver, B. Schulte, F.-U. Stein, T. Matsuyama, G. Jotzu, G. Meier, and A. Cavalleri, Light-induced anomalous Hall effect in graphene, Nat. Phys. **16**, 38 (2020).

[99] K. Wintersperger, C. Braun, F. N. Ünal, A. Eckardt, M. D. Liberto, N. Goldman, I. Bloch, and M. Aidelsburger, Realization of an anomalous Floquet topological system with ultracold atoms, Nat. Phys. **16**, 1058 (2020).

[100] S. Mukherjee, A. Spracklen, M. Valiente, E. Andersson, P. Öhberg, N. Goldman, and R. R. Thomson, Experimental observation of anomalous topological edge modes in a slowly driven photonic lattice, Nat. Commun. **8**, 13918 (2017).

[101] L. J. Maczewsky, J. M. Zeuner, S. Nolte, and A. Szameit, Observation of photonic anomalous Floquet topological insulators, Nat. Commun. **8**, 13756 (2017).

[102] Q. Cheng, Y. Pan, H. Wang, C. Zhang, D. Yu, A. Gover, H. Zhang, T. Li, L. Zhou, and S. Zhu, Observation of anomalous π modes in photonic Floquet engineering, Phys. Rev. Lett. **122**, 173901 (2019).